

# Chapter 2

## Opacity modelling of low series members for population and emergent flux calculations : The escape probability and absorption factor approach

### 2.1 Introduction

This chapter describes the theory for modelling opacity in low series members using the escape factor approach, and its application as the code ADAS 214. Two quantities are evaluated, the escape probability ( $\Theta$ ) for emergent flux adjustments and the absorption factor ( $\Lambda$ ) for population modifications, see equations (1.8) and (1.14) of chapter 1.

ADAS 214 is derivative of the work of Behringer who developed a code for the practical evaluation of (1.8) and (1.14). This chapter outlines the theory behind the new ADAS code, highlighting the various approximations which are made. The original Behringer code was used in the study of an air-like plasma jet (Jentschke, 1995), then amended and extended with a later version being used to account for opacity in low temperature

divertor plasmas (Behringer, 1997). The original code was written in BASIC for DOS, and later translated to Visual Basic for WINDOWS 95 by Behringer. The code was converted to run as an ADAS code, referred to as ADAS 214 (see Summers, 2001 and the original report of Behringer, 1998). ADAS 214 consists of an IDL graphical interface which spawns a fortran 77 code to evaluate the  $\Lambda$  and  $\Theta$  expressions. Figure 2.1 shows the processing options screen where the plasma parameters are entered. The code also requires an input ‘adf04’ file containing all the A-values, collisional rates etc for the ion under consideration.

The code outputs an opacity modified version of this file, with the A-values adjusted by the appropriate absorption factors. This file can be used in collisional-radiative calculations to produce an optically thick population distribution. ADAS 214 has two main graphical outputs, it shows the generic  $\Lambda$  and  $\Theta$  curves with selected transitions marked (as in figure 1.11) as well as plotting line ratios verses column density (as in figure 1.12).

## 2.2 Basic Theory

In the evaluation of  $\Theta$  and  $\Lambda$  expressions, considerable simplification is possible with the assumption of certain geometries and spatial distribution of the emission coefficient. The geometries considered by the code are:

- Isotropic sphere of radius  $b$ .
- Plane parallel disk of thickness  $2b$ .
- Cylinder with radius  $b$  and length  $2a$ .

See figures 2.2 and 2.3 for the details of these geometries. The escape probability is evaluated on a line of sight through the centre of the sphere, along the central axis of the disk and perpendicular to the central axis of the cylinder. The absorption factor is evaluated at the centre of the sphere and at the midpoint of the central axis of both the disk and the cylinder (note that the absorption factor evaluated in the code is only valid at this point).

ADAS214 PROCESSING OPTIONS

Data File Name:  
/packages/adas/adf04/cophath/cophath\_bnt97b.dat  
Browse Comments

Atomic Mass Number: 1

Select Line profile:  Doppler  Lorentzian  Holtsmark  Double Doppler  Voigt  Doppler-Holtsmark

Select Density distribution:  Homogeneous  Linear  Parabolic

Select Plasma geometry:  Sphere  Disk  Cylinder

Scan?  Yes  No  
No. of steps: 14  
Min factor: 0.10 Max factor: 2.50

Density (cm<sup>-3</sup>): 1.0000e+14  
Dimension(b) (cm): 7.50000

Ion Temp (K): 23010.0  
Boltz. E-Temp (K): 11605.0  
Aspect ratio (a/b): 5.00000

Observed spectrum lines

INDEX	Upper level N	Lower level N
1	2	1
2	3	1
3	4	1
4	5	1
5	3	2

Edit Table

Note: max allowed N quantum no. :  
min allowed N quantum no. :

Designate metastables and Boltzmann deviations  
Enter a multiplier for each metastable  
(press return after each entry)

1 n=1	(2)0( 0.5)	0.0 (1)1.000	1.000
2 n=2	*(2)0( 3.5)	82259.0 (1)1.000	
3 n=3	*(2)0( 8.5)	97492.0 (1)1.000	
4 n=4	*(2)0(15.5)	102824.0 (1)1.000	
5 n=5	*(2)0(24.5)	105292.0 (1)1.000	

Cancel Done

Figure 2.1: Example of the processing options screen in ADAS 214. Note the range of plasma parameters which need to be entered, in particular the Boltzmann deviation factor that it used in the initial population estimation.

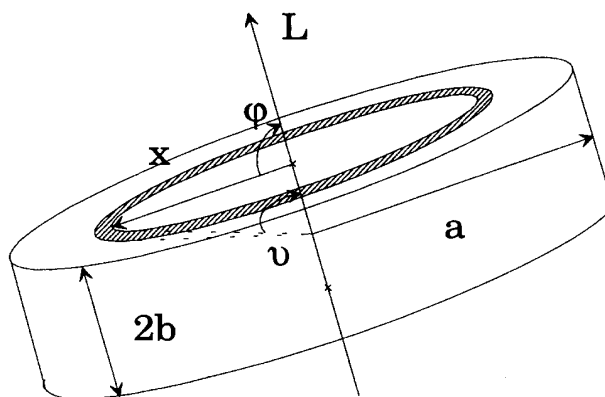


Figure 2.2: Schematics of the disk geometry considered by ADAS 214, taken from the report of Behringer (1998).

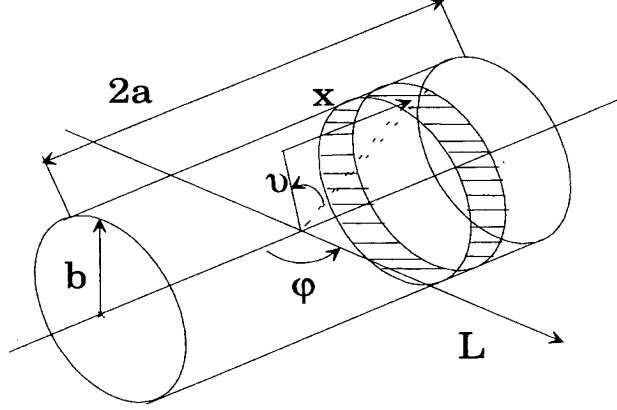


Figure 2.3: Schematics of the cylindrical geometry considered by ADAS 214, taken from the report of Behringer (1998).

Consider first the escape probability expression from chapter one:

$$\Theta = \frac{\int_{line} \int_0^{2b} \varepsilon(\nu, l) e^{-\int_l^{2b} \alpha(\nu, l') dl'} dl d\nu + \int_{line} I(\nu, 0) e^{-\int_0^{2b} \alpha(\nu, l) dl} d\nu}{\int_{line} \int_0^{2b} \varepsilon(\nu, l) dl d\nu} \quad (2.1)$$

Assume that there is no background radiation field ( $I(\nu, 0) = 0$ ) and that  $\alpha$  is independent of spatial position within the plasma and equal to  $\bar{\alpha}(\nu)$ . The assumption of constant absorption coefficient represents the main approximation in the code, equivalent to assuming a constant lower level population density throughout the plasma volume. This should be a reasonable approximation for fusion divertor conditions and for many low temperature plasmas. Opacity effects are commonly investigated in transitions with either the ground or metastables as their lower level. Because of the large populations of these levels it should be valid to assume that they are spatially invariant. The escape probability is then given by

$$\begin{aligned} \Theta &= \frac{\int_{line} \int_0^{2b} \varepsilon(\nu, l) e^{-\int_l^{2b} \bar{\alpha}(\nu) dl'} dl d\nu}{\int_{line} \int_0^{2b} \varepsilon(\nu, l) dl d\nu} \\ &= \frac{\int_{line} \int_0^{2b} \varepsilon(\nu, l) e^{(l-2b)\bar{\alpha}(\nu)} dl d\nu}{\int_{line} \int_0^{2b} \varepsilon(\nu, l) dl d\nu} \end{aligned} \quad (2.2)$$

Define  $\varepsilon_L(l)$  such that emission coefficient can be written as

$$\begin{aligned}
\varepsilon(\nu, l) &= \frac{1}{4\pi} A_{n' \rightarrow n} N_{n'}(l) \theta(\nu) \\
&= \varepsilon_L(l) \theta(\nu)
\end{aligned} \tag{2.3}$$

and  $\bar{\alpha}_L$  such that

$$\begin{aligned}
\bar{\alpha}(\nu) &= N_n \frac{c^2}{8\pi} \left( \frac{n'}{n} \right)^2 \frac{1}{\nu_{n' \rightarrow n}^2} A_{n' \rightarrow n} \theta(\nu) \\
&= \bar{\alpha}_L \theta(\nu)
\end{aligned} \tag{2.4}$$

Assuming that the emission and absorption line profiles are independent of position, the escape probability can be written as

$$\Theta = \frac{\int_0^{2b} \varepsilon_L(l) \int_{line} \theta(\nu) e^{(l-2b)\bar{\alpha}_L \theta(\nu)} d\nu dl}{\int_0^{2b} \varepsilon_L dl} \tag{2.5}$$

Consider next the absorption factor expression, starting with equation (1.14).

$$\Lambda(l) = 1 - \frac{\int_{\Omega} \int_{line} \alpha(\nu, l) u(\nu, l) d\nu d\Omega}{\int_{\Omega} \int_{line} \varepsilon(\nu, l) d\nu d\Omega} \tag{2.6}$$

Again, one assumes that the absorption coefficient is independent of  $l$ . For the purposes of the code  $\Lambda$  is evaluated at the centre of our plasma geometry, denoted by  $l=b$ . It is assumed that emission from this point is uniform in all directions (i.e.  $\int_{\Omega} \int_{line} \varepsilon(\nu, l) d\nu d\Omega = 4\pi\varepsilon_L$ ). Thus

$$\Lambda(b) = 1 - \frac{\bar{\alpha}_L \int_{\Omega} \int_{line} \theta(\nu) u(\nu, b) d\nu d\Omega}{4\pi\varepsilon_L} \tag{2.7}$$

The radiation field term is given by

$$u(\nu) = \int_{h(\Omega)}^b \varepsilon_L(l) \theta(\nu) e^{(l-b)\bar{\alpha}_L \theta(\nu)} dl \tag{2.8}$$

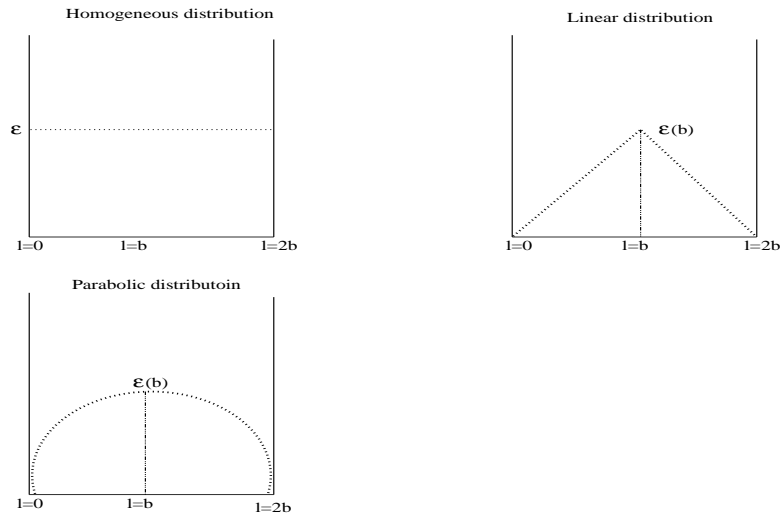


Figure 2.4: Diagrams of the spatial distribution of the emission coefficient as considered by ADAS 214.

with  $h(\Omega)$  describing a point on the plasma surface. Thus the radiation field is the resultant radiation, incident from all possible lines of sight into the centre, accounting for attenuation along each line of sight.

Note that equation (2.8) is similar to the numerator of the equation (2.5), allowing one to significantly simplify the numerics of the calculation. As will be seen in the next section, the emergent flux along a given line of sight can be expressed purely as a function of optical depth. Thus  $u(\nu)$  can be evaluated for a range of optical depths, used immediately to evaluate  $\Theta$  and called repeatedly in the solid angle integration for  $\Lambda$ . Thus it is only necessary to work out the generic  $u(\nu)$  vs  $\tau$  curve once and the rest of the calculations can be performed from interpolation of these results.

## 2.3 Spatial variation in the emission coefficient

The code allows for various distributions in the emission coefficient within the volume of the plasma. These options are

- homogeneous distribution throughout the plasma.
- linear decrease from plasma centre to edge.
- parabolic decrease from plasma centre to edge.

Writing out the intensity expression and repeatedly integrating by parts results in

$$\begin{aligned}
 I(\nu, b) &= \int_0^b \varepsilon(\nu, l) e^{(l-b)\bar{\alpha}(\nu)} dl \\
 &= \frac{\varepsilon(\nu, b)}{\bar{\alpha}(\nu)} - \frac{\varepsilon'(\nu, b)}{\bar{\alpha}(\nu)^2} + \frac{\varepsilon''(\nu, b)}{\bar{\alpha}(\nu)^3} - \dots \\
 &\quad - e^{-\bar{\alpha}(\nu)b} \left[ \frac{\varepsilon(\nu, 0)}{\bar{\alpha}(\nu)} - \frac{\varepsilon'(\nu, 0)}{\bar{\alpha}(\nu)^2} + \frac{\varepsilon''(\nu, 0)}{\bar{\alpha}(\nu)^3} - \dots \right]
 \end{aligned} \tag{2.9}$$

The variation in the allowed emission coefficient distributions is at most second order making this technique an efficient way of evaluating the line of sight integration. When this expression is evaluated for each emission coefficient distribution, the following expressions are achieved (results with the integration extending from  $0 \rightarrow 2b$  and from  $0 \rightarrow b$  are shown since they are used in the calculation of  $\Theta$  and  $\Lambda$  respectively): For the homogeneous distribution one has

$$\begin{aligned}
 \int_0^b \varepsilon(\nu, l) e^{(l-b)\bar{\alpha}(\nu)} dl &= \frac{\varepsilon(\nu)}{\bar{\alpha}(\nu)} [1 - e^{-\bar{\alpha}(\nu)b}] \\
 \int_0^{2b} \varepsilon(\nu, l) e^{(l-2b)\bar{\alpha}(\nu)} dl &= \frac{\varepsilon(\nu)}{\bar{\alpha}(\nu)} [1 - e^{-2\bar{\alpha}(\nu)b}]
 \end{aligned} \tag{2.10}$$

For the linear distribution these become

$$\begin{aligned}
 \int_0^b \varepsilon(\nu, l) e^{(l-b)\bar{\alpha}(\nu)} dl &= \frac{\varepsilon(\nu, b)}{\bar{\alpha}(\nu)} \left[ 1 - \frac{1}{\bar{\alpha}(\nu)b} + \frac{1}{\bar{\alpha}(\nu)b} e^{-\bar{\alpha}(\nu)b} \right] \\
 \int_0^{2b} \varepsilon(\nu, l) e^{(l-2b)\bar{\alpha}(\nu)} dl &= \frac{\varepsilon(\nu, b)}{\bar{\alpha}(\nu)} \frac{1}{\bar{\alpha}(\nu)b} \left[ 1 - 2e^{-\bar{\alpha}(\nu)b} + e^{-2\bar{\alpha}(\nu)b} \right]
 \end{aligned} \tag{2.11}$$

and

$$\begin{aligned}\int_0^b \varepsilon(\nu, l) e^{(l-b)\bar{\alpha}(\nu)} dl &= \frac{\varepsilon(\nu, b)}{\bar{\alpha}(\nu)} \left[ 1 - \frac{2}{\bar{\alpha}(\nu)^2 b^2} + \left( \frac{2}{\bar{\alpha}(\nu)b} + \frac{2}{\bar{\alpha}(\nu)^2 b^2} \right) e^{-\bar{\alpha}(\nu)b} \right] \\ \int_0^{2b} \varepsilon(\nu, l) e^{(l-2b)\bar{\alpha}(\nu)} dl &= \frac{\varepsilon(\nu, b)}{\bar{\alpha}(\nu)} \frac{1}{\bar{\alpha}(\nu)b} \left[ 2 - \frac{2}{\bar{\alpha}(\nu)b} + \left( 2 + \frac{2}{\bar{\alpha}(\nu)b} \right) e^{-2\bar{\alpha}(\nu)b} \right]\end{aligned}\quad (2.12)$$

for the parabolic distribution. This results in escape and absorption factor expressions of

$$\begin{aligned}\Theta &= \int_{line} \frac{\theta(\nu)[1 - e^{-2\bar{\alpha}(\nu)b}]}{2\bar{\alpha}(\nu)b} d\nu \\ &= \int_{line} \frac{\theta(\nu)[1 - e^{-2\tau(\nu)}]}{2\tau(\nu)} d\nu \\ \Lambda(b) &= \frac{1}{4\pi} \int_{\Omega} \int_{line} \theta(\nu) e^{-\bar{\alpha}(\nu)b(\Omega)} d\nu d\Omega \\ &= \frac{1}{4\pi} \int_{\Omega} \int_{line} \theta(\nu) e^{-\tau(\nu, \Omega)} d\nu d\Omega\end{aligned}\quad (2.13)$$

for the homogeneous distribution.

$$\begin{aligned}\Theta &= 2 \int_{line} \frac{1}{\bar{\alpha}(\nu)b} \theta(\nu) \frac{1}{\bar{\alpha}(\nu)b} \left[ 1 - 2e^{-\bar{\alpha}(\nu)b} + e^{-2\bar{\alpha}(\nu)b} \right] d\nu \\ &= 2 \int_{line} \frac{1}{\tau(\nu)} \theta(\nu) \frac{1}{\tau(\nu)} \left[ 1 - 2e^{-\tau(\nu)} + e^{-2\tau(\nu)} \right] d\nu \\ \Lambda(b) &= \frac{1}{4\pi} \int_{\Omega} \int_{line} \left[ \frac{1}{\bar{\alpha}_L b(\Omega)} - \frac{1}{\bar{\alpha}_L b(\Omega)} e^{-\bar{\alpha}(\nu)b(\Omega)} \right] d\nu d\Omega \\ &= \frac{1}{4\pi} \int_{\Omega} \int_{line} \left[ \frac{\theta(\nu)}{\tau(\nu, \Omega)} - \frac{\theta(\nu)}{\tau(\nu, \Omega)} e^{-\tau(\nu, \Omega)} \right] d\nu d\Omega\end{aligned}\quad (2.14)$$

for the linear distribution and

$$\Theta = \frac{3}{4} \int_{line} \left[ \frac{1}{\bar{\alpha}(\nu)b} \theta(\nu) \frac{1}{\bar{\alpha}(\nu)b} \left[ 2 - \frac{2}{\bar{\alpha}(\nu)b} + \left[ 2 + \frac{2}{\bar{\alpha}(\nu)b} \right] e^{-2\bar{\alpha}(\nu)b} \right] \right] d\nu$$

$$\begin{aligned}
&= \frac{3}{4} \int_{line} \left[ \frac{1}{\tau(\nu)} \theta(\nu) \frac{1}{\tau(\nu)} \left[ 2 - \frac{2}{\tau(\nu)} + \left[ 2 + \frac{2}{\tau(\nu)} \right] e^{-2\tau(\nu)} \right] \right] d\nu \\
\Lambda(b) &= \frac{1}{2\pi} \int_{\Omega} \int_{line} \left[ \frac{2}{(\bar{\alpha}(\nu)b(\Omega))(\bar{\alpha}b(\Omega))} - \left[ \frac{2}{\bar{\alpha}_L b(\Omega)} + \frac{2}{(\bar{\alpha}(\nu)b(\Omega))(\bar{\alpha}_L b(\Omega))} \right] \right. \\
&\quad \left. e^{-\bar{\alpha}(\nu)b(\Omega)} \right] d\nu d\Omega \\
&= \frac{1}{2\pi} \int_{\Omega} \int_{line} \left[ \frac{2\theta(\nu)}{(\tau(\nu, \Omega))^2} - \left[ \frac{2\theta(\nu, \Omega)}{\tau(\nu, \Omega)} + \frac{2\theta(\nu)}{(\tau(\nu, \Omega))^2} \right] e^{-\tau(\nu, \Omega)} \right] d\nu d\Omega \quad (2.15)
\end{aligned}$$

for the parabolic distribution. Each of these expressions are functions of optical depth ( $\bar{\alpha}_L b$ ) and line profile, allowing generic  $\Theta$  and  $\Lambda$  vs  $\tau$  curves to be evaluated, see figure 2.5.

## 2.4 Proof that generic $\Lambda(b)$ and $\Theta$ vs optical depth curves are valid

The code evaluates the escape and absorption factor expression as generic curves that are only functions of optical depth. The optical depth for each possible transition is then worked out and its corresponding escape and absorption factor found by interpolation of the generic curve. Thus the generic curve is assumed to be valid for every possible transition within the one ion. It is not immediately obvious that this approach is valid. There are two issues to be dealt with, firstly can the expression always be written in terms of optical depth and secondly how does one account for the fact that different transitions can have different line profiles?

To show that the expressions can always be written in terms of optical depth consider the following argument: By inspection from equations (2.10) - (2.15) it can be seen that  $\Theta$  and  $\Lambda$  can be written in terms of optical depth and line profile. It can be shown that this is generally the case if one writes the emission coefficient with the spatial variation extracted, that is  $\varepsilon(\nu, l) = \varepsilon(\nu, b)f(l)$  where  $f(l)$  defines the variation of  $\varepsilon$  along  $l$ . It has been shown in equations (2.10) - (2.15) that the line integrated flux can be written as  $\frac{\varepsilon(\nu, b)}{\bar{\alpha}(\nu)} g(\tau(\nu), \theta(\nu))$  where  $g$  is the appropriate function from these equations. The escape and absorption factors can then be written.

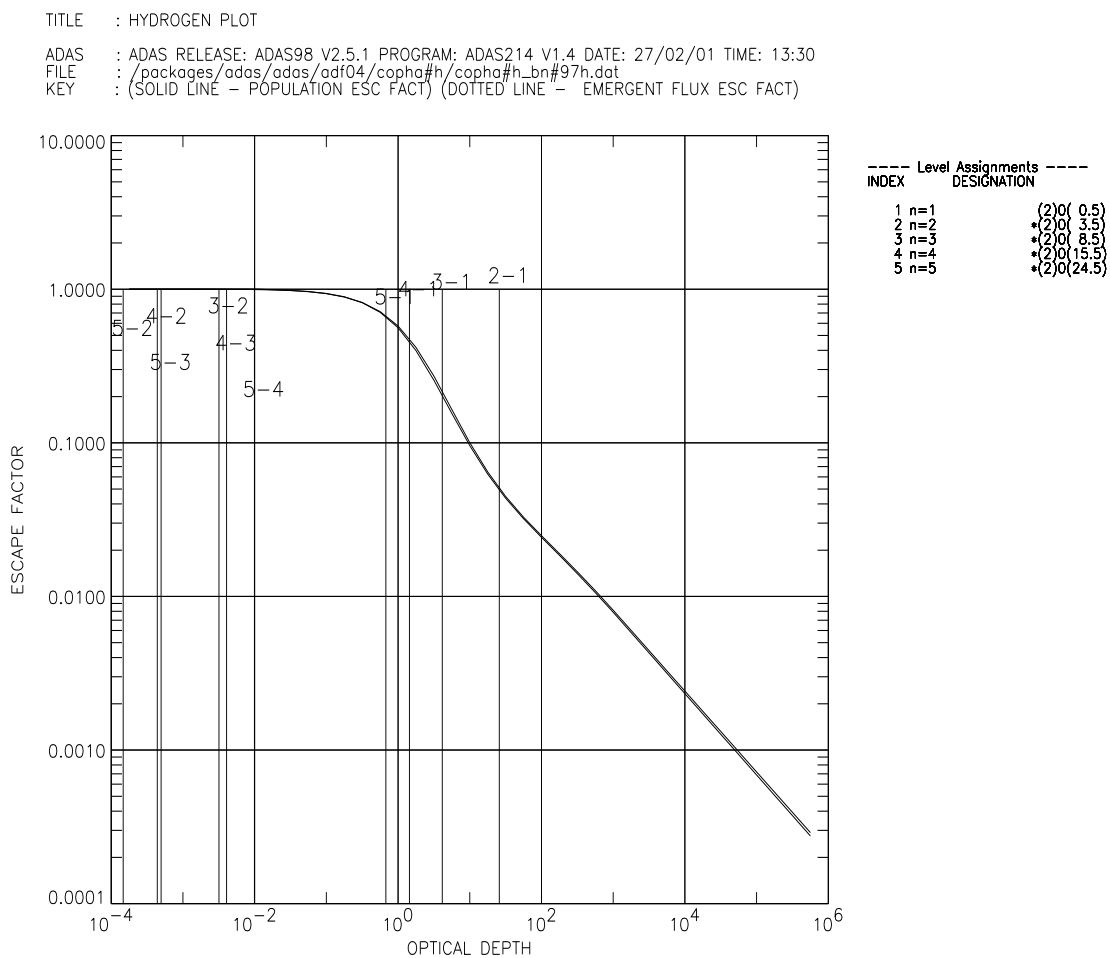


Figure 2.5: Example of the generic  $\Theta$  and  $\Lambda$  curves produced by ADAS 214. Note that as one progresses up a given series the  $\Theta$  and  $\Lambda$  values increase. The  $\Theta$  and  $\Lambda$  values also increase from one series to the next

$$\begin{aligned}
\Theta &= \frac{\int_0^b \int_{line} \varepsilon(\nu, l) e^{(l-b)\alpha(\nu)} d\nu dl}{\int_0^b \int_{line} \varepsilon(\nu, l) d\nu dl} \\
&= \frac{\int_0^b f(l) \int_{line} \varepsilon(\nu, b) e^{(l-b)\alpha(\nu)} d\nu dl}{\int_0^b f(l) dl \int_{line} \varepsilon(\nu, b) d\nu dl} \\
&= \frac{\int_0^b f(l) \int_{line} \frac{\varepsilon(\nu, b)}{\bar{\alpha}(\nu)} g(\tau(\nu), \theta(\nu)) d\nu dl}{\int_0^b f(l) dl \int_{line} \varepsilon_L(b) \theta(\nu) d\nu dl} \\
&= \frac{\varepsilon_L(b) \int_0^b f(l) \int_{line} \frac{\theta(\nu)}{\bar{\alpha}(\nu)} g(\tau(\nu), \theta(\nu)) d\nu dl}{\varepsilon_L(b) \int_0^b f(l) dl \int_{line} \theta(\nu) d\nu dl} \\
&= \frac{\int_0^b f(l) \int_{line} \frac{1}{\bar{\alpha}_L} g(\tau(\nu), \theta(\nu)) d\nu dl}{\int_0^b f(l) dl} \tag{2.16}
\end{aligned}$$

$$\begin{aligned}
\Lambda(b) &= 1 - \frac{\int_{\Omega} \int_{line} \bar{\alpha}(\nu) u(\nu, b) d\nu d\Omega}{\int_{\Omega} \int_{line} \varepsilon(\nu, b) d\nu d\Omega} \\
&= 1 - \frac{\int_{\Omega} \int_{line} \bar{\alpha}(\nu) \frac{\varepsilon(\nu, b)}{\bar{\alpha}(\nu)} g(\tau(\nu, \Omega), \theta(\nu)) d\nu d\Omega}{\int_{\Omega} \int_{line} \varepsilon_L(b) \theta(\nu) d\nu d\Omega} \\
&= 1 - \frac{\varepsilon_L(b) \int_{\Omega} \int_{line} \theta(\nu) g(\tau(\nu, \Omega), \theta(\nu)) d\nu d\Omega}{\varepsilon_L(b) 4\pi} \\
&= \frac{\int_{\Omega} \int_{line} \theta(\nu) g(\tau(\nu, \Omega), \theta(\nu)) d\nu d\Omega}{4\pi} \tag{2.17}
\end{aligned}$$

Thus, for a given line profile, one can generate generic  $\Theta$  and  $\Lambda$  vs optical depth curves. It should be noted that for both  $\Theta$  and  $\Lambda$  a normalised line profile is used with the actual line height contained in the  $\varepsilon_L$  term. Provided that the same normalised profile holds for all transitions, the generic  $\Theta$  and  $\Lambda$  vs  $\tau$  curve will hold for each transition. This is likely to be the case as it is mainly adjacent series members with either the ground or a metastable as the lower level that are optically thick. The same broadening mechanisms are likely to apply to such lines giving them similar profiles. The higher series transitions, which are more likely to have different profiles,

are often optically thin, but even if they are not thin they have little effect on the population results of the code.

## 2.5 Profile Theory

Dealing next with the various line profile options, there are three basic profiles, and three convolved profiles allowed for in the code, namely

- Doppler
- Lorentzian
- Holtsmark
- Voigt
- Doppler-Holtsmark
- Double Doppler

Normalised profiles are generated numerically in the code from expressions such as those in section 1.2.5. The Doppler half-widths are determined from expression (1.26), the Lorentzian and Holtsmark widths are set to half the Doppler width and for the convolved profiles, the non-Doppler width is entered by the user.

The integration over the wavelength is performed numerically, at this point the escape probability can be found from expression (2.5).

## 2.6 Evaluation of $\Lambda$

To evaluate the absorption factor, it is necessary to integrate over solid angle, so knowledge of the plasma geometry is required. This integration is performed numerically. For the spherical geometry  $\Lambda$  can be returned immediately with the solid angle integration introducing a factor of  $4\pi$ . For the cylinder and disk geometries the

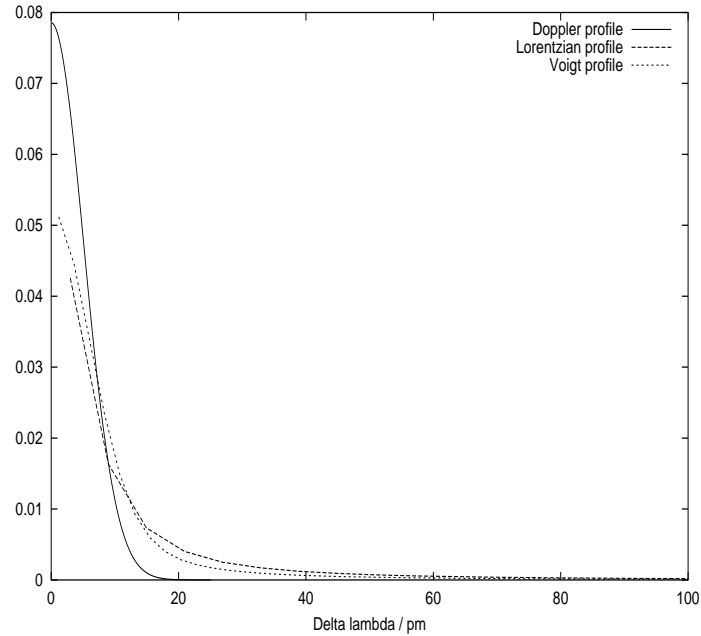


Figure 2.6: Example of various hydrogen profiles as calculated by ADAS 214. Note that all profiles are normalised and evaluated for the same set of plasma parameters. The Lorentzian width is set to half the doppler width as is the Lorentzian component of the voigt profile.

symmetry of the problem is exploited in that it is only necessary to evaluate the contribution from one strip. An element of surface area is considered along a given strip and its contribution to the radiation field at  $b$  evaluated. The contribution from each element along the strip is then worked out, with an end correction used to account for the flat ends of both geometries.

## 2.7 Computation of populations using absorption factors

The main purpose of the code is to allow opacity modified population distributions to be evaluated within ADAS collisional-radiative codes. These codes assemble all the collisional, radiative and spontaneous rates between atomic levels, and then solve the system to predict a population structure. The individual rates are either evaluated from algebraic expressions or taken from the best available observational/calculated

data. One type of input datafile is known as an adf04 file, these optically thin datafiles can be converted to account for opacity effects using ADAS 214. This is done automatically in the code, each transition being read in from the input file, its A-value modified by the appropriate  $\Lambda$  and written to the output ‘optically thick’ adf04 file. All of the existing ADAS codes assume that the plasma is optically thin, thus the absorption factor technique of modifying the Einstein A-values with  $\Lambda$  factors is ideal in that it allows the ‘optically thin’ collisional-radiative codes to process opacity modified adf04 files and generate a thick population structure.

## 2.8 Using the code as a line ratio diagnostic

ADAS 214 has an extension from the original code which allows the user to specify a range of column densities for which to run the absorption factor calculation. The code then evaluates absorption factors for each column density, producing corresponding adf04 files and opacity modified population distributions (via ADAS 214’s own statistical balance subroutine). It is then a small matter to look up the escape probability expression at each column density for two chosen transitions and use equation (1.46) to work out the opacity modified line ratio. Thus one can evaluate any given emergent flux line ratio as a function of column density. See figure 2.7 for an example of this. The modified populations which are evaluated are for one point in the plasma and it is assumed that they remain constant along the line of sight. This is not entirely consistent with the selection of a modified upper level density distribution in the absorption factor calculation. That is, the upper level population modification is taken into account in the evaluation of  $\Lambda$  and  $\Theta$ , but not in the  $N_{n'}$  used in the emergent flux calculation. Within this limitation the line ratio option of the code can provide an estimate of any given ratio for immediate comparison with observational data. Alternatively the user can evaluate the modified population density along the line of sight themselves and perform the integrated flux and hence line ratio calculation themselves.

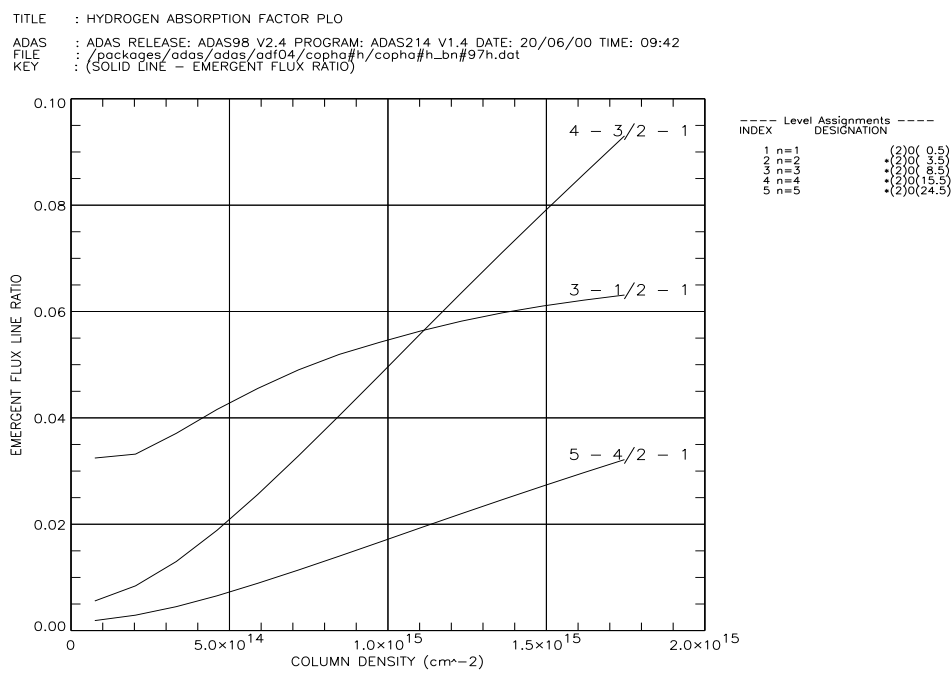


Figure 2.7: Example of the emergent flux line ratio evaluation vs column density from ADAS 214. The ratios are evaluated for hydrogen with the indexes corresponding to upper and lower principal quantum numbers. The plasma parameters are those from the fusion divertor study of section 1.3.2

## 2.9 Example of the use of the code for He line identification using CDS quiet sun observations

A useful illustration of ADAS 214 is found in part of the spectral line identification work of Brooks et al. (1999). In this study the Coronal Diagnostic Spectrometer (CDS) instrument onboard the SOHO spacecraft was used to obtain a complete spectrum of the quiet sun using the instrument's full wavelength range (308 – 381Å, 513 – 633Å), the aim being to identify as many spectral lines as possible. An example of an observed spectral region is shown in figure 2.8 with some of the line identifications marked. Strict criteria were used in the identification of the lines. Firstly wavelength coincidence with accepted values was considered, and for lines where this coincidence was good, 'position patterns' could be used to confirm an identification. These position patterns refer to a technique first introduced in the analysis of data for the Spacelab 2 CHASE experiment in Lang, Mason & McWhirter (1990) and elaborated in Brooks et al. (1999). Spectra were taken over a range of spatial and temporal points and assigned a unique position index. Thus the different observations reflect typical quiet sun variabilities in density, temperature, structure. Each spectral line is then reduced to a single value by taking its intensity in counts divided by its average over all positions. These points are then plotted logarithmically against position index. When the position patterns for identified lines are arranged in order of similar patterns, and labelled with the ions temperature (from the peak of its  $G(T_e)$ ), it is found that there are similar patterns for lines emitted by the same ion and for lines from ions formed at approximately the same temperature. Thus the position patterns of unidentified lines can act as a fingerprint indicating the probable temperature of formation of the line, thus aiding in its identification. It was sometimes possible to use line intensity ratios to judge whether or not lines originated from the same emitting ion and in this way further confirm certain identifications. A brief description is presented below on the use of ADAS 214 in aiding in the identification of four He I lines.

From wavelength coincidence and the similarities of their position plots, it was strongly suspected that four observed lines were

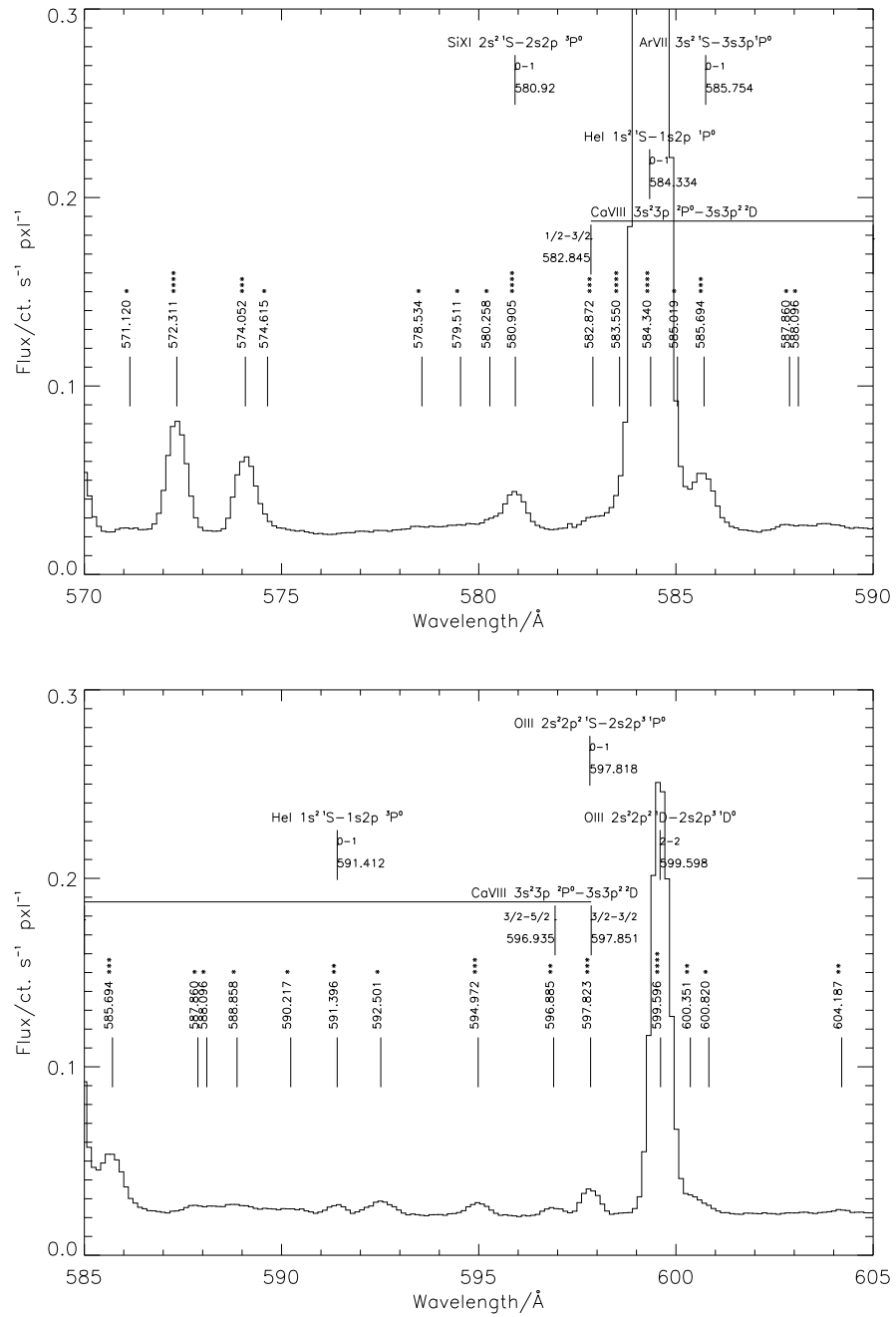


Figure 2.8: Example of the observed CDS spectrum used in the line identification work, taken from Brooks et al. (1999).

- He I  $1s^2\ ^1S_0 - 1s4p\ ^1P_1$  522.257Å
- He I  $1s^2\ ^1S_0 - 1s3p\ ^1P_1$  537.091Å
- He I  $1s^2\ ^1S_0 - 1s2p\ ^1P_1$  584.360Å
- He I  $1s^2\ ^1S_0 - 1s2p\ ^3P_1$  591.411Å

The 522, 537, and 584 lines were all strong and there was no doubt about their identification (see figure 2.8 upper plot for the 584 line), in fact these lines were used as calibration lines in the study. The 591 intercombination line on the other hand was very weak (see figure 2.8 lower plot) and evidence of the consistency of the observed intensities was needed for a definite identification. The observed line intensity ratios of each line to the 584 line intensity are shown in column two of table 2.1. Also shown is the predicted optically thin intensity ratio (column three) where the populations were evaluated from ADAS. It can be seen that the observed  $I(537)/I(584)$  and  $I(522)/I(584)$  ratios lie close to their optically thin values, while the  $I(591)/I(584)$  ratio significantly deviates from it. It would be expected that the strong lines (584, 537 and 522) would be optically thick and so have a reduced emergent flux from the sun. If they have similar opacities they may experience similar intensity reductions, moving their ratios back to the expected thin values.

To see if opacity could explain the deviation of the  $I(591)/I(584)$  ratio from that observed, ADAS 214 was used to return opacity and line ratio estimates. A disk geometry was chosen with a large aspect ratio to simulate a near infinite slab for the solar atmosphere. Doppler profiles were used along with a homogeneous density distribution, with the temperature being taken as 28,000K from the peak of the  $G(T_e)$  function, see figure 2.9. A helium density of  $1 \times 10^{10} \text{cm}^{-3}$  was taken from the corresponding value in the Vernazza et al (1981) solar atmosphere model, assuming that the helium density to be ten percent of the hydrogen density. The length of the slab was judged approximately from the height from the photosphere to the transition region, again taken from the Vernazza model. The input adf04 file was generated using the autostructure code via the ADAS 701 interface. An A-value for the intercombination line of  $0.6 \text{s}^{-1}$  was taken from Summers (1977).

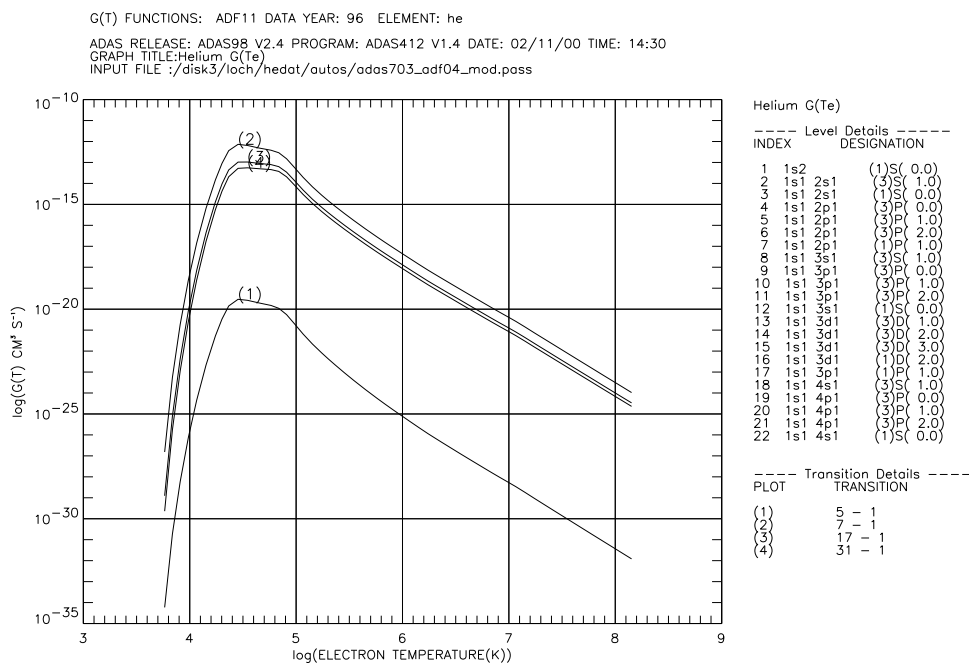


Figure 2.9:  $G(T_e)$  function for helium evaluated using ADAS 412; note that the peak of the  $G(T_e)$  lies at about 28,000K.

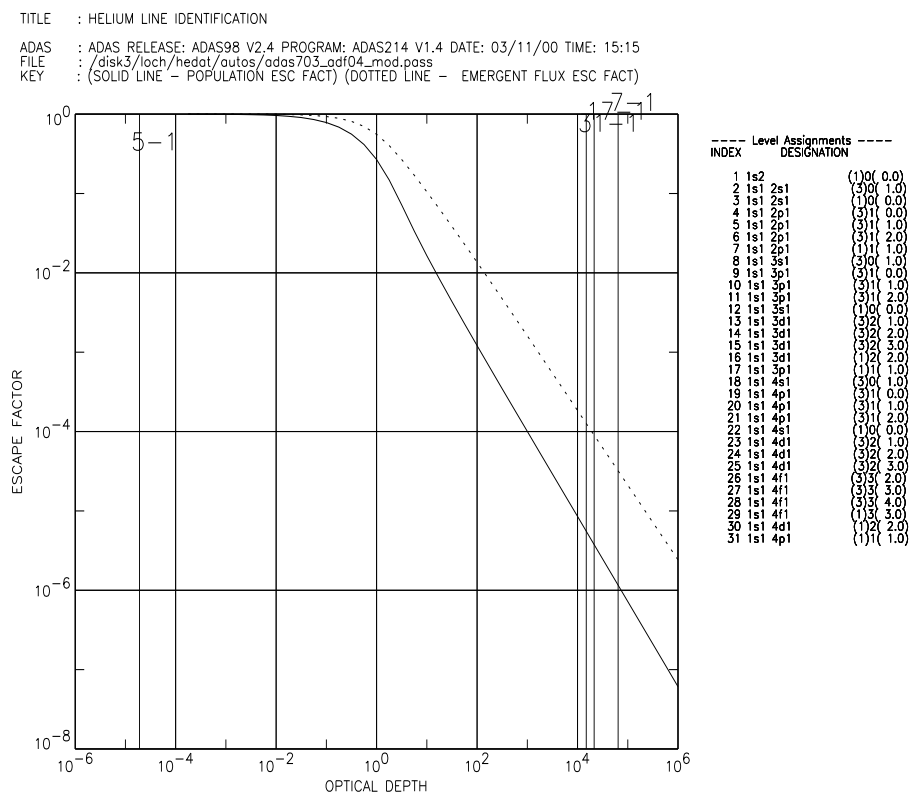


Figure 2.10: Escape factor plot generated using ADAS 214 for the helium line identification work.

TITLE : HELIUM LINE IDENTIFICATION

ADAS : ADAS RELEASE: ADAS98 V2.4 PROGRAM: ADAS214 V1.4 DATE: 04/11/00 TIME: 16:11  
 FILE : /disk3/loch/hedat/autos/adas703\_adf04\_mod.pass  
 KEY : (SOLID LINE - EMERGENT FLUX RATIO)

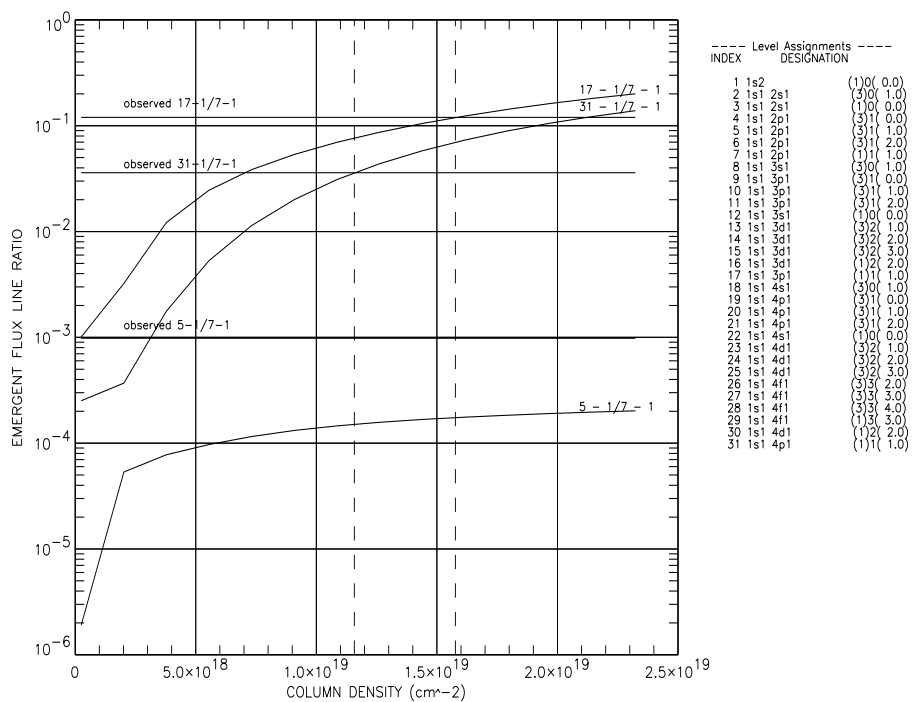


Figure 2.11: Line ratio plot generated using ADAS 214 for the helium line identification work.

Using these values an escape factor calculation was performed. The results are shown in figures 2.10 and 2.11. The 584, 537 and 522 lines are clearly extremely optically thick. Note that they have similar opacities, thus their ratios should be close to the optically thin values (i.e. their intensities scale similarly with optical depth so their ratios can still remain close to the optically thin ratio, even though the individual lines are optically thick). The 591 line on the other hand can be seen to be optically thin, and so the observed deviation from the thin line is to be expected. So a quick assessment of the escape probabilities using ADAS 214 has qualitatively explained the observed ratios.

The intensity ratios were then estimated - note that a ratio analysis like this is not the main purpose of the code, since the evaluated absorption factor is only valid at the centre of the geometry under investigation and the ratio evaluation assumes that it is valid for the whole line of sight. Despite this it was useful to estimate the ratios within the bounds of the code to get an indication of their behaviour. A range of column densities surrounding the value for which figure 2.10 was generated were chosen and the ratios produced. The results are shown in figure 2.11. Note that both the  $I(537)/I(584)$  and  $I(522)/I(584)$  cross their observed values at approximately the same column density ( $\approx 1.3 \times 10^{19} \text{ cm}^{-2}$ ). The  $I(591)/I(584)$  on the other hand does not reach its observed value, always lying below it. This is not unexpected as we are running the code in the regime beyond which it is normally valid. The predicted  $I(591)/I(584)$  ratio is too low, indicating that we have overestimated the  $I(584)$  intensity. As a result of this analysis it was decided to run the MULTI radiative transfer stellar atmosphere code (Carlson, 1986) to predict the line ratios. This approach is more likely to give a better estimate of the line ratios than ADAS 214 as it uses a solar atmosphere model based geometry and density distribution (in the case here the model of Vernazza et al., 1981). MULTI was run and line ratios produced - see column four of table 2.1. As can be seen from the table the predicted ratios are good for both the  $I(537)/I(584)$  and  $I(522)/I(584)$  ratios. The optically thick model matches the  $I(591)/I(584)$  ratio better than the thin model, though it is still a little low.

As a result of this analysis the line was positively identified as  $HeI 1s^2 \ ^1S_0 - 1s2p \ ^3P_1$

Ratio	Measured	Predicted Ratio	
		Opt. thin ratio	MULTI ratio
I(537)/I(584)	$(1.2 \pm 0.3) \times 10^{-1}$	$(0.6 - 1.3) \times 10^{-1}$	$(1.5) \times 10^{-1}$
I(522)/I(584)	$(3.6 \pm 1.0) \times 10^{-2}$	$(1.8 - 4.2) \times 10^{-2}$	$(5.9) \times 10^{-2}$
I(591)/I(584)	$(9.8 \pm 3.2) \times 10^{-4}$	$(1.0 - 1.8) \times 10^{-4}$	$(4.3) \times 10^{-4}$

Table 2.1: Observed and calculated solar atmosphere helium line ratios with and without the effects of opacity.

591.411Å. To the author's knowledge this line has not been observed before in the sun. The short illustration shown here provides a good example of the use of ADAS 214 for more complex problems than its assumptions might allow. The code provides a means of quickly estimating the opacity effects on spectral lines of moderately optically thick plasmas, and if the lines are found to fall outside of the optical depths for which the code is valid, it allows the investigator to decide whether it is worthwhile doing a more complex opacity study on the lines in question, as was done in this case.

## 2.10 Further theory and code development : Inclusion of a background radiation field

### 2.10.1 Theory

One of the first assumptions made in evaluating the escape and absorption factor expression was the exclusion of a background radiation field. Expressions (2.10) through to (2.14) can be re-evaluated to include a contribution from the background radiation field. Note that the parabolic expression is not included in the work shown here, though it is straightforward to extend the algebra to allow for it.

For the homogeneous distribution the line integrated fluxes become

$$\int_0^b \varepsilon(\nu, l) e^{(l-b)\bar{\alpha}(\nu)} dl = \frac{\varepsilon(\nu)}{\bar{\alpha}(\nu)} [1 - e^{-\bar{\alpha}(\nu)b}] + I(\nu, 0) e^{-\bar{\alpha}(\nu)b}$$

$$\int_0^{2b} \varepsilon(\nu, l) e^{(l-2b)\bar{\alpha}(\nu)} dl = \frac{\varepsilon(\nu)}{\bar{\alpha}(\nu)} \left[ 1 - e^{2\bar{\alpha}(\nu)b} \right] + I(\nu, 0) e^{-\bar{\alpha}(\nu)2b} \quad (2.18)$$

and

$$\begin{aligned} \int_0^b \varepsilon(\nu, l) e^{(l-b)\bar{\alpha}(\nu)} dl &= \frac{\varepsilon(\nu, b)}{\bar{\alpha}(\nu)} \left[ 1 - \frac{1}{\bar{\alpha}(\nu)b} + \frac{1}{\bar{\alpha}(\nu)b} e^{-\bar{\alpha}(\nu)b} \right] + I(\nu, 0) e^{-\bar{\alpha}(\nu)b} \\ \int_0^{2b} \varepsilon(\nu, l) e^{(l-2b)\bar{\alpha}(\nu)} dl &= \frac{\varepsilon(\nu, b)}{\bar{\alpha}(\nu)} \frac{1}{\bar{\alpha}(\nu)b} \left[ 1 - 2e^{-\bar{\alpha}(\nu)b} + e^{-2\bar{\alpha}(\nu)b} \right] + I(\nu, 0) e^{-\bar{\alpha}(\nu)2b} \end{aligned} \quad (2.19)$$

for the linear distribution.

These result in escape and absorption factors expressions for a homogeneous density distribution of

$$\begin{aligned} \Theta &= \frac{1}{2b\varepsilon_L + \int_{line} u_{BB}(\nu) d\nu} \int_{line} \left[ \frac{\varepsilon_L}{\bar{\alpha}_L} \left[ 1 - e^{-2\bar{\alpha}(\nu)b} \right] + u_{BB}(\nu) e^{-2\bar{\alpha}(\nu)b} \right] d\nu \\ \Lambda(l) &= \frac{2}{4\pi} \int_{\Omega} \int_0^{\infty} \left[ \theta(\nu) e^{-\bar{\alpha}(\nu)b(\Omega)} - \frac{\bar{\alpha}(\nu)}{\varepsilon_L} u_{BB}(\nu) e^{-\bar{\alpha}(\nu)b(\Omega)} \right] d\nu d\Omega \end{aligned} \quad (2.20)$$

and

$$\begin{aligned} \Theta &= \frac{1}{b\varepsilon_L + 2 \int_{line} u_{BB}(\nu) d\nu} \\ &\quad \times \left[ 2 \int_{line} \frac{\varepsilon(\nu, b)}{\bar{\alpha}(\nu)} \frac{1}{\bar{\alpha}(\nu)b} \left[ 1 - 2e^{-\bar{\alpha}(\nu)b} + e^{-2\bar{\alpha}(\nu)b} \right] + u_{BB}(\nu) e^{-2\bar{\alpha}(\nu)b} \right] d\nu \\ \Lambda(l) &= \frac{2}{4\pi} \int_{\Omega} \int_0^{\infty} \left[ \left( \frac{1}{\bar{\alpha}_L b(\Omega)} - \frac{1}{\bar{\alpha}_L b(\Omega)} e^{-\bar{\alpha}_L b(\Omega)} \right) - \right. \\ &\quad \left. \frac{\bar{\alpha}(\nu)}{\varepsilon_L(b)} u_{BB}(\nu) e^{-\bar{\alpha}(\nu)b(\Omega)} \right] d\nu d\Omega \end{aligned} \quad (2.21)$$

for a linear density distribution, where  $u_{BB}(\nu)$  is the incident background radiation density at frequency  $\nu$ . A modified version of ADAS 214 was produced to account for such a background field. Although the resultant escape probabilities were found

to be well behaved, it proved to be difficult to evaluate meaningful absorption factors for all possible optical depths. For example, consider the case of a plasma that shows only moderate opacity and has an incident background radiation field which is close to black body. Due to the low opacity of the plasma, the radiation field at the center will be close to black body (mostly due to the background field). Note from the absorption factor expressions (2.20) and (2.21) that the multiplier on  $u_{BB}$  is  $\alpha/\varepsilon$ . If the background radiation density is black body, one only gets  $\lambda = 0$  if  $\alpha$  and  $\varepsilon$  have Boltzmann populations. However, the code assumes an initial excited state population structure with default Boltzmann deviation factors of 0.1 (with the option for the user to enter a different deviation factor). This serves to increase  $\alpha/\varepsilon$ , allowing the background field contribution to  $\lambda$  to become less than negative one, resulting in negative absorption factors. If the system were allowed to iterate then the large radiation field would increase the population of the excited states and keep the absorption factors positive. Since the direction of the present work seeks to exploit the linear nature of the escape factor approach no further work was done on this aspect.

## 2.11 Conclusions

A description of the ADAS 214 opacity code has been given and it can be seen that it integrates well with the existing ADAS collisional-radiative codes. It provides a quick and effective way of evaluating opacity adjustments to both atomic populations and emergent flux from moderately optically thick plasmas.